

Efficient moment-based approach to the simulation of infinitely many heterogeneous phase oscillators

Iván León¹ and Diego Pazó¹

Instituto de Física de Cantabria (IFCA), Universidad de Cantabria-CSIC, Avda. Los Castros, s/n, 39005 Santander, Spain

(Dated: 19 May 2022)

The dynamics of ensembles of phase oscillators are usually described considering their infinite-size limit. In practice, however, this limit is fully accessible only if the Ott-Antonsen theory can be applied, and the heterogeneity is distributed following a rational function. In this work we demonstrate the usefulness of a moment-based scheme to reproduce the dynamics of infinitely many oscillators. Our analysis is particularized for Gaussian heterogeneities, leading to a Fourier-Hermite decomposition of the oscillator density. The Fourier-Hermite moments obey a set of hierarchical ordinary differential equations. As a preliminary experiment, the effects of truncating the moment system and implementing different closures are tested in the analytically solvable Kuramoto model. The moment-based approach proves to be much more efficient than the direct simulation of a large oscillator ensemble. The convenience of the moment-based approach is exploited in two illustrative examples: (i) the Kuramoto model with bimodal frequency distribution, and (ii) the ‘enlarged Kuramoto model’ (endowed with nonpairwise interactions). In both systems we obtain new results inaccessible through direct numerical integration of populations.

A wide variety of systems can be modeled as ensembles of oscillators, from biological systems (e.g. neuronal networks) to physical ones (e.g. power grids). Their cooperative phenomena, e.g. collective synchronization, are often described in terms of interacting (one-dimensional) phase oscillators. The dynamics of globally coupled phase oscillators, initiated long ago by Winfree¹ and Kuramoto², is a vibrant topic of nonlinear science³. Considering infinitely many phase oscillators (the so-called thermodynamic limit) is a key assumption to make useful theoretical and phenomenological descriptions. In practice, however, simulations are customarily carried out with large ensembles of oscillators, assuming they faithfully reflect what even larger populations do. This straightforward approach may be inconvenient for two reasons: its inaccuracy due to finite-size fluctuations, and its computational cost due to the trigonometric functions involved. The situation is even more pressing when collective chaos (or hyperchaos) is found, since microscopic chaos contributes with a macroscopic amount of positive Lyapunov exponents⁴, possibly masking the actual value of the collective exponents. In this work, we study a moment-based scheme for systems of infinitely many heterogeneous oscillators. The moment system is the result of decomposing the oscillator density in a basis of Fourier components and orthonormal polynomials. This decomposition appeared some years ago in a paper by Chiba⁵, although only recently it demonstrated its utility to address numerical issues⁶. In this work, we first test the moment-based approach with the Kuramoto model. We compare different closures of the moment system. The moment-based approach proves to be highly efficient in general. In the second part of this paper, we carry out moment-based simulations in two illustrative systems, obtaining new results hardly achievable through the direct numerical simulation of phase oscillators. In particular, unstable solutions can be continued uncovering in this way a previously unnoticed bifurcation, and “collective” Lyapunov exponents

are obtained at a relatively low computational cost.

I. INTRODUCTION

Self-sustained oscillators pervade the natural world and our technology-driven society. The synchronization between them (spiking cells, electronic/microwave circuits, etc.) is conspicuous⁷. Ultimately, this is the consequence of natural evolution or technical design. Though under certain circumstances synchronization may also be an indicator of malfunction.

From a mathematical perspective, the dynamics on a limit-cycle attractor can be parametrized by a cyclic coordinate, called the phase. Under weak disturbances, a perturbative technique, called phase reduction, permits to eliminate all degrees of freedom except the phase^{2,8}. This automatically suggests using the phase oscillator as the natural unit to describe weakly interacting limit-cycle oscillators.

Collective synchronization is typical in large ensembles of oscillators. Classical examples include cardiac pacemaker cells in the sinoatrial node⁹, swarms of flashing fireflies¹⁰, arrays of Josephson junctions¹¹, to cite a few¹². Populations of heterogeneous phase oscillators reproduce the onset of collective synchronization, as originally proven in a seminal numerical experiment by Winfree¹³. Some years later Kuramoto derived a tractable model¹⁴, subsequently used as building block to investigate a variety of collective phenomena: chimera states¹⁵, gamma oscillations in the brain¹⁶, swarming^{17,18}, etc. Nowadays, the dynamics of populations of phase oscillators continue attracting the interest of an interdisciplinary community of scientists^{3,19}.

The theoretical efforts to describe populations of globally coupled phase oscillators usually adopt the thermodynamic limit, i.e. the population size N is assumed to be infinite (with the coupling strength scaling as $1/N$). This simplification is, for instance, part of the original Kuramoto’s self-

consistent analysis¹⁴, the stability analysis of incoherence by Strogatz and Mirrollo²⁰, and the Ott-Antonsen theory²¹. In practice, we can generally regard the dynamics of a large population of phase oscillators as an ideal infinite population, plus small finite-size fluctuations vanishing in the thermodynamic limit. Altogether, theoretical approaches and phenomenological characterizations routinely refer to the infinite-size limit.

In some special cases, the dynamics of infinitely many oscillators can be reduced to a few ordinary differential equations (ODEs). In technical terms, this is possible when the ‘‘Ott-Antonsen manifold’’ is attracting^{21,22}, and the heterogeneity is represented by a rational probability density function (e.g. Lorentzian). Otherwise, the standard procedure to explore the thermodynamic limit is simulating increasingly larger population sizes. As we will show below this strategy is, however, not optimal and potentially inaccurate. It is not optimal due to unavoidable finite-size fluctuations, and the computational cost of the trigonometric functions involved. Furthermore, within this strategy, unstable collective states are hardly accessible, and the stability of attracting states is poorly estimated.

The situation is even worse if the collective dynamics is chaotic. Direct numerical simulations may turn to be completely insufficient. The actual value of the Lyapunov exponents in the thermodynamic limit may be masked by an $O(N)$ amount of positive Lyapunov exponents⁴. We have recently found such a problem in a population of phase oscillators with pairwise and nonpairwise interactions⁶.

The drawbacks of direct numerical simulations were already tackled in the context of the Kuramoto model²³ (KM). The first step was to consider an infinite population from the outset, and thereby working with the oscillator density. The most promising methodology is the moment-based approach, initially proposed in Ref.²⁴. Here we start from a decomposition of the oscillator density first proposed by Chiba⁵. In his work, the set of moments was used as an instrument to prove that in the KM the limit $N \rightarrow \infty$ is well behaved. In a recent paper⁶, we found that the moments defined in⁵ serve as convenient variables for numerical simulations. In this work, our aims are (i) to analyze this moment-based approach in detail (assessing the performance of different closures in the KM), and (ii) to use moments in a couple of relevant problems (clearly outperforming direct simulations).

The remainder of this paper is structured as follows. In Sec. II we present the family of phase oscillator network models under study. In Sec. III we introduce the moment-based approach, and derive the evolution equation of a set of Fourier-Hermite moments. The accuracy of the moment system in the solvable case of the KM is investigated in Sec. IV. Sections V and VI demonstrate the might of the moment-based approach with two examples: the KM with bimodal frequency distribution, and the ‘‘enlarged KM’’ (a system with nonpairwise interactions). Finally, in Sec. VII we recapitulate our main results and suggest possible extensions of this work.

II. GLOBALLY COUPLED PHASE OSCILLATORS

A phase oscillator is a dynamical system described solely by one cyclic variable, the phase $\theta \in [0, 2\pi)$. As already discussed above, the study of large ensembles of globally coupled phase oscillators constitute a popular branch of non-linear science³. These dynamical systems evolve in an N -dimensional torus $\{\theta_j\}_{j=1,2,\dots,N}$, and are particularly difficult to analyze if heterogeneity is present. Specifically, we consider a family of systems, whose deterministic evolution equations are:

$$\dot{\theta}_j = \sigma \omega_j + G(\theta_j, t). \quad (1)$$

Here the overdot denotes the time derivative. The ω_j are drawn from a probability distribution $g(\omega)$, which is centered at zero without lack of generality. The form of Eq. (1) is shared, among others, by the well-known Kuramoto-Daido system^{2,25} and the Winfree model¹³. In both situations function G exclusively encodes the coupling between the oscillators, plus a frequency offset Ω_0 . Therefore $\sigma \omega_j$ are the deviations from the central natural frequency of the oscillators. In a more general setup, function G may include the nonuniformity of the rotations, as in ensembles of active rotators²⁶ (derived from a periodically forced KM). We abuse of language and refer to G as the coupling function hereafter. In function G the time dependence may enter explicitly, and implicitly through the Kuramoto-Daido order parameters^{14,25}: $Z_k(t) = \frac{1}{N} \sum_j e^{ik\theta_j}$, $k = 1, 2, \dots$. For example, the KM corresponds to $G(\theta, t) = \Omega_0 + \varepsilon \text{Im}[Z_1(t)e^{-i\theta}]$, where ε is the coupling constant.

For convenience $g(\omega)$ is chosen to possess unit variance, such that parameter σ in Eq. (1) controls the dispersion. In this work we adopt the normal distribution $\omega_j \sim \mathcal{N}(0, 1)$, i.e. the probability density function is:

$$g(\omega) = \frac{1}{\sqrt{2\pi}} e^{-\omega^2/2}. \quad (2)$$

Other distributions with finite moments can, in principle, be analyzed in an analogous way, as discussed in Sec. VII.

III. THEORY

A. Continuous formulation

The dynamics of large systems of the form (1) is usually described assuming the thermodynamic limit, $N \rightarrow \infty$. It is seldom proven⁵, but usually assumed, that for sufficiently large system sizes the dynamics is simply that of the thermodynamic limit, supplemented by irrelevant, asymptotically small, finite-size fluctuations²⁷. Still, the analysis of the thermodynamic limit of Eq. (1) is not trivial in general. The only analytically solvable situation is that in which G contains only the first harmonic in θ (often expressed as $G(\theta, t) = \text{Im}[H(t)e^{-i\theta}]$), and $g(\omega)$ is a rational function. The dynamics becomes exactly described by a few ODEs inside the Ott-Antonsen manifold²¹ (but not the transient from an arbitrary initial condition).

Simulating Eq. (1) for an increasing number of oscillators may give an idea of the asymptotic dynamics in the thermodynamic limit. Alternatively, we may choose to start the analysis in the thermodynamic limit, defining a conditional oscillator density $\rho(\theta|\omega, t)$ such that $\rho(\theta|\omega, t)g(\omega)d\theta d\omega$ is the fraction of oscillators with phases between θ and $\theta + d\theta$ and “pseudo-frequencies” between ω and $\omega + d\omega$ at time t . The density ρ obeys the continuity equation:

$$\frac{\partial \rho}{\partial t} = -\frac{\partial}{\partial \theta} \{[\sigma\omega + G(\theta, t)]\rho\}. \quad (3)$$

A variety of approaches have been proposed in order to efficiently solve the previous equation, specially in the context of the KM, see Sec. VI.B in²³.

B. Pérez-Vicente and Ritort’s moments

The moment-based approach was inaugurated in 1997 by Pérez-Vicente and Ritort²⁴. They put forward a set of modes H_k^m , where k and m are integers ($m \geq 0$). In terms of the oscillator density

$$H_k^m(t) = \int_0^{2\pi} d\theta e^{ik\theta} \int_{-\infty}^{\infty} d\omega g(\omega) \omega^m \rho(\theta|\omega, t). \quad (4)$$

The hierarchical set of ODEs governing the moments H_k^m can be obtained from Eq. (3). This numerical scheme was successfully tested in²⁴ with the Kuramoto model with a bi-delta distribution of natural frequencies (and white noise, which is trivially incorporated, see Sec. VII). Its performance with a continuous frequency distribution remains, to our knowledge, unknown.

C. Chiba’s moments: Orthonormal polynomials

Another moment system was introduced by Chiba⁵ in 2013, with the aim of proving that the dynamics of the N -dimensional Kuramoto model converges to the continuous model as $N \rightarrow \infty$. In Ref.⁵ the moments were defined as

$$P_k^m(t) = \int_0^{2\pi} d\theta e^{ik\theta} \int_{-\infty}^{\infty} d\omega g(\omega) h_m(\omega) \rho(\theta|\omega, t). \quad (5)$$

Instead of powers of ω , as in (4), now the definition in (5) includes a function $h_m(\omega)$, which is one element of the orthonormal set of polynomials satisfying

$$\int_{-\infty}^{\infty} h_m(\omega) h_n(\omega) g(\omega) d\omega = \delta_{m,n}. \quad (6)$$

For Gaussian $g(\omega)$, the appropriate basis is formed by the probabilist’s Hermite polynomials (rescaled by $\sqrt{m!}$): $h_m(x) = \text{He}_m(x)/\sqrt{m!}$. The conditional oscillator density is expanded in the basis of the Fourier-Hermite modes (5) as follows:

$$\rho(\theta|\omega, t) = \frac{1}{2\pi} \sum_{k=-\infty}^{\infty} \sum_{m=0}^{\infty} P_k^m(t) e^{-ik\theta} h_m(\omega). \quad (7)$$

The Fourier-Hermite modes P_k^m appear to be particularly convenient. They are the extension of the Kuramoto-Daido order parameters to the space of the natural frequencies. In particular, $P_k^0 = Z_k$ in the thermodynamic limit. Moreover, $P_0^m = \delta_{m,0}$, in contrast to the analogous modes H_0^m in (4), which are nonzero. This implies that in a uniform incoherent state (UIS), $\rho = 1/(2\pi)$, the only nonzero moment is $P_0^0 = 1$.

D. Evolution equation of the Fourier-Hermite modes

The ODEs governing the dynamics of the P_k^m modes are obtained inserting (7) into the continuity equation (3). As a preliminary step, we write the Fourier decomposition of the coupling function $G(\theta, t)$:

$$G(\theta, t) = \frac{1}{2\pi} \sum_{l=-\infty}^{\infty} G_l(t) e^{-il\theta} \quad (8)$$

where $G_l = G_{-l}^*$, as G is a real-valued function. The right-hand side of (3) yields two terms. The first one is:

$$\frac{\partial(\sigma\omega\rho)}{\partial\theta} = -\frac{i\sigma}{2\pi} \sum_{k,m} k e^{-ik\theta} P_k^m [\sqrt{m}h_{m-1} + \sqrt{m+1}h_{m+1}], \quad (9)$$

where we have used the recurrence relation $\omega h_m(\omega) = \sqrt{m}h_{m-1}(\omega) + \sqrt{m+1}h_{m+1}(\omega)$. The second term in (3) is:

$$\frac{\partial(G\rho)}{\partial\theta} = \frac{-i}{2\pi} \sum_{k,m,l} (k+l) e^{-i(k+l)\theta} G_l P_k^m h_m. \quad (10)$$

Collecting terms accompanying $e^{-ik\theta} h_m(\omega)$ at both sides of Eq. (3), we get:

$$\frac{1}{k} \dot{P}_k^m = i\sigma \left(\sqrt{m}P_k^{m-1} + \sqrt{m+1}P_k^{m+1} \right) + i \sum_{l=-\infty}^{\infty} P_{k-l}^m G_l, \quad (11)$$

where it is implicit that $P_{-k}^m = (P_k^m)^*$. For clarity, we can split the last sum in the previous equation:

$$\begin{aligned} \frac{1}{k} \dot{P}_k^m = i\sigma \left(\sqrt{m}P_k^{m-1} + \sqrt{m+1}P_k^{m+1} \right) \\ + iP_k^m G_0 + \sum_{l=1}^{\infty} iP_{k+l}^m G_l^* + iP_{k-l}^m G_l. \end{aligned} \quad (12)$$

This equation becomes slightly simplified rotating each moment by $-\pi m/2$ radians:

$$P_k^m = (-i)^m P_k^m. \quad (13)$$

Then, the resulting system of complex-valued ODEs reads

$$\begin{aligned} \frac{1}{k} \dot{P}_k^m = \sigma \left(\sqrt{m}P_k^{m-1} - \sqrt{m+1}P_k^{m+1} \right) \\ + iP_k^m G_0 + \sum_{n=1}^{\infty} iP_{k+n}^m G_n^* + iP_{k-n}^m G_n. \end{aligned} \quad (14)$$

This infinite set of ODEs exactly describes the dynamics of (3). In the limit $\sigma \rightarrow 0$, the modes decouple in the index m , and the dynamics is fully described by the subset $P_k^0 = Z_k$, i.e. the usual Fourier modes for a homogeneous system²⁸.

E. Closure

Equation (14) is useful as long as working with a finite number of moments in the numerical simulation is able to reproduce the dynamics of the oscillator ensemble, Eq. (1). The expectation is that (with a suitable truncation) Eq. (14) should capture the thermodynamic limit of (1) better than a direct simulation of a large number of oscillators. In the latter case finite-size fluctuations systematically deteriorate the results.

We restrict here to rectangular truncations of the modes, i.e. we neglect all the modes with $k > k_{\max}$ and $m > m_{\max}$. Therefore, we are confronted with dynamical systems of dimension $2 \times k_{\max} \times (m_{\max} + 1)$. In practical terms, the values of k_{\max} and m_{\max} are selected as a trade-off between the numerical accuracy and the computational capabilities. For the problems treated in this paper, the terms G_l in the Fourier expansion of G beyond $|l| = 1$ or 2 vanish. Then, values of k_{\max} and m_{\max} of the order of a few tens are typically enough, while keeping reasonable running times in a desktop computer. Physical considerations may require to increase k_{\max} or m_{\max} . For instance, if the system exhibits a very coherent state $|Z_1| \approx 1$ the value of k_{\max} may need to be larger. In addition, m_{\max} may need to be increased if the dynamics becomes particularly complex.

The second point to be addressed is the boundary condition imposed when truncating Eq. (14). Concerning the index k , we simply impose $P_{k_{\max}+1}^m = 0$, in analogy to the condition used for homogeneous systems²⁸. For the index m choosing a suitable closure is not obvious. As shown below, imposing $P_k^{m_{\max}+1} = 0$ yields inconsistent results. We are therefore impelled to refine the closure. A constant boundary condition $P_k^{m_{\max}+1} = P_k^{m_{\max}}$, or a linear extrapolation

$$P_k^{m_{\max}+1} = 2P_k^{m_{\max}} - P_k^{m_{\max}-1} \quad (15)$$

are obvious candidates. In general, we can take an extrapolation of $P_k^{m_{\max}+1}$ using a polynomial function of degree n_a . The general formula is

$$P_k^{m_{\max}+1} = \sum_{n=1}^{n_a+1} \binom{n_a+1}{n} (-1)^{(n+1)} P_k^{m_{\max}-n+1}, \quad (16)$$

where $n_a = 0, 1, 2,$ and 3 correspond to constant, linear, quadratic, and cubic degrees, respectively.

IV. KURAMOTO MODEL WITH GAUSSIAN FREQUENCY DISTRIBUTION

The KM with unimodal frequency distribution is a paradigmatic example of globally coupled oscillator system, which is analytically solvable to a large extent. We resort to it as a preliminary testbed system, where Eq. (14) and their closures in Eq. (16) can be examined in detail.

As already advanced, in the KM the interaction function is:

$$G(\theta, t) = \varepsilon R \sin(\Psi - \theta) = \frac{\varepsilon}{2i} (Z_1 e^{-i\theta} - Z_1^* e^{i\theta}), \quad (17)$$

where $Z_1 \equiv R e^{i\Psi}$ is the Kuramoto order parameter, and the central frequency Ω_0 was set equal to zero by going to a rotating frame. At low couplings, $0 < \varepsilon < \varepsilon_c$, the KM exhibits the uniform incoherent state (UIS), characterized by a uniform oscillator density. In the UIS all Kuramoto-Daido order parameters vanish, $Z_k = 0$ (in the thermodynamic limit, otherwise fluctuations around zero survive). Above the critical coupling, $\varepsilon > \varepsilon_c$, a state of partial synchrony (PS) spontaneously sets in. In the state of PS a macroscopic cluster of oscillators becomes phase-locked, and $Z_k \neq 0$ accordingly.

With the interaction function in Eq. (17), Eq. (14) governing the evolution of the Fourier-Hermite modes becomes:

$$\frac{1}{k} \dot{P}_k^m = \sigma \left(\sqrt{m} P_k^{m-1} - \sqrt{m+1} P_k^{m+1} \right) + \frac{\varepsilon}{2} \left(P_{k+1}^m Z_1^* - P_{k-1}^m Z_1 \right). \quad (18)$$

A. Critical coupling

As a first test, we check if Eq. (18) with different closures is able to reproduce the instability of incoherence at the critical coupling ε_c . With Gaussian $g(\omega)$, Eq. (2), the critical coupling satisfies $\varepsilon_c/\sigma = \sqrt{8/\pi} = 1.595769\dots$

We linearize Eq. (14) around the UIS, corresponding to $P_k^m = \delta_{k,0} \delta_{m,0}$. Only the modes with $k = 1$ may destabilize. The corresponding (linearized) ODEs read:

$$\dot{P}_1^m = \sigma \left(\sqrt{m} P_1^{m-1} - \sqrt{m+1} P_1^{m+1} \right) - \frac{\varepsilon}{2} \delta_{m,0} P_1^0. \quad (19)$$

The critical coupling ε_c at which one eigenvalue of the Jacobian matrix crosses zero depends on m_{\max} and on the boundary condition. The null ‘‘boundary condition’’ $P_1^{m_{\max}+1} = 0$ turns out to be inadequate, since then the critical coupling is predicted to be zero, irrespective of the value of m_{\max} . For other choices, see Eq. (16), the value of ε_c converges to the exact result as m_{\max} grows. In Fig. 1(a) we may see that the value of $\varepsilon_c(m_{\max})$ converges to the asymptotic value in a non-monotonic way. The larger the degree of the polynomial extrapolation (n_a), the faster the convergence, see Fig. 1(b). Empirically, we find the power-law convergence $|\Delta\varepsilon_c| \equiv |\varepsilon_c - \varepsilon_c(m_{\max})| \propto (m_{\max})^{-n_a-1}$. In the N -dimensional KM the convergence is comparatively slower with the number of degrees of freedom: the onset of entrainment spreads over a distance $\delta\varepsilon_c \sim N^{-2/5}$ for randomly sampled natural frequency distribution²⁹, while $\delta\varepsilon_c \sim N^{-4/5}$ for deterministic samplings³⁰.

B. Partially synchronized state

The analytical tractability of the KM permits to obtain the exact values of the Fourier-Hermite modes in the PS state. We use them as a reference for comparing the accuracy of different truncations and closures of the moment system. We restrict our study to a specific coupling above criticality $\varepsilon/\sigma =$

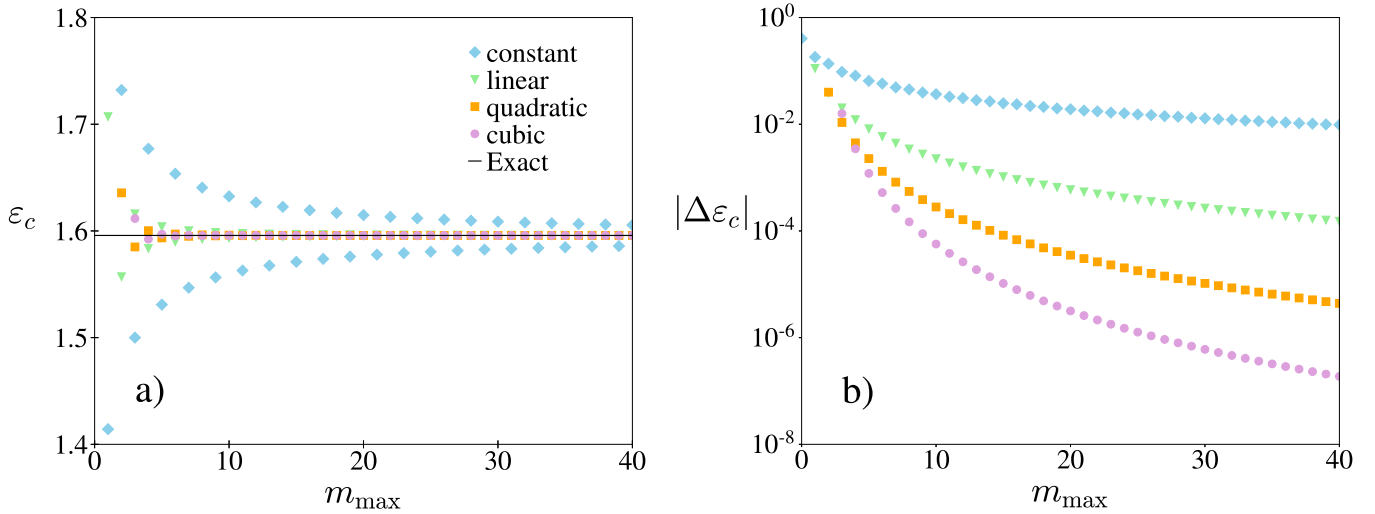


FIG. 1. (a) Instability threshold of incoherence ε_c for the moment system (18) as a function of m_{\max} ($\sigma = 1$). Four different polynomial closures are considered: $n_a = 0$, constant; $n_a = 1$, linear; etc. The exact value of ε_c in the thermodynamic limit is marked by a horizontal solid line. (b) Log-linear plot of the deviation from the exact result for the data sets in panel (a).

1.8. The stationary density of PS can be written as a Fourier expansion

$$\rho(\theta|\omega) = \frac{1}{2\pi} + \frac{1}{2\pi} \left[\sum_{k=1}^{\infty} \alpha(\omega)^k e^{-ik\theta} + \text{c.c.} \right], \quad (20)$$

where c.c. stands for complex conjugate. The coefficients are $\alpha(\omega)^k$, as noted by Ott and Antonsen when their ansatz was proposed²¹. Function α is piecewise defined distinguishing between oscillators locked to the mean field and drifting oscillators ($\sigma = 1$ is adopted hereafter):

$$\alpha(\omega) = \begin{cases} \sqrt{1 - \frac{\omega^2}{\varepsilon^2 R^2}} + i \frac{\omega}{\varepsilon R} & \text{if } |\omega| \leq \varepsilon R \\ \frac{i\omega}{\varepsilon R} \left(1 - \sqrt{1 - \frac{\varepsilon^2 R^2}{\omega^2}} \right) & \text{if } |\omega| \geq \varepsilon R \end{cases} \quad (21)$$

where we have chosen a reference frame such that $Z_1 = R > 0$. As a preliminary step, we determined R solving the self-consistency condition³¹ $R = \int_{-\infty}^{\infty} d\omega g(\omega) \alpha(\omega)$. Now the Fourier-Hermite modes are obtained from Eq. (5) integrating the powers of $\alpha(\omega)$

$$P_k^m(t) = \int_{-\infty}^{\infty} d\omega g(\omega) h_m(\omega) \alpha(\omega)^k. \quad (22)$$

The numerical evaluation of the integral in Eq. (22) yields the exact values of the Fourier-Hermite mode P_k^m (we did not cast the solution in terms of non-elementary functions). For the specific coupling constant $\varepsilon = 1.8$, the absolute values of the modes with $m = 0$ are depicted in Fig. 2(a) by a solid black line. The magnitudes of the modes eventually decrease at an exponential rate with k . For other values of m (not shown), the exponential regime is reached after an initial growth at small k values. The dependence of the modes on the index m is more convoluted. Figure 2(b) shows, as a solid line, the representative case $k = 1$. The decay with index m exhibits

damped oscillations, and an envelope decaying as a stretched exponential $e^{-b\sqrt{m}}$ according to our numerical exploration.

Figure 2 also shows the Fourier-Hermite modes obtained as the fixed point of (18) with four different closures, and two different system sizes ($k_{\max} = m_{\max} = 20$ or 40.) A Newton-Raphson algorithm was used to locate the fixed point in each case. (The result agrees with the attracting resting state observed simulating Eq. (18).) As occurred with the critical coupling, the larger the degree of the polynomial extrapolation, the more accurate the results are. In Fig. 2(b) only the constant boundary condition appreciably deviates from the exact result. The linear extrapolation (15) is used in the rest of the paper as it represents a good tradeoff between accuracy and simplicity. The quadratic and cubic boundary conditions have proven to be more accurate so far. However, this advantage—proven for time-independent quantities—may not materialize when (complex) dynamics arise, due to the risk of overfitting.

In Fig. 2, the number of modes (20×20 or 40×40) appears not to be very relevant. This somewhat unexpected conclusion deserves to be analyzed systematically. We conclude this section with an extensive exploration of the impact of k_{\max} and m_{\max} . In Fig. 3, the error of the modulus of the Kuramoto-Daido order parameters $|Z_1| = |P_1^0|$ and $|Z_7| = |P_7^0|$, for different configurations of k_{\max} and m_{\max} , are depicted in color scale. The figure shows that a minimum number of modes in k and m are needed to obtain a reliable result. With a few hundred modes ($m_{\max} > k_{\max} \sim 20$) the errors already become quite small. The figure clearly confirms that the error eventually decreases upon increasing k_{\max} and m_{\max} (though in a specific, non-monotonic fashion for each mode).

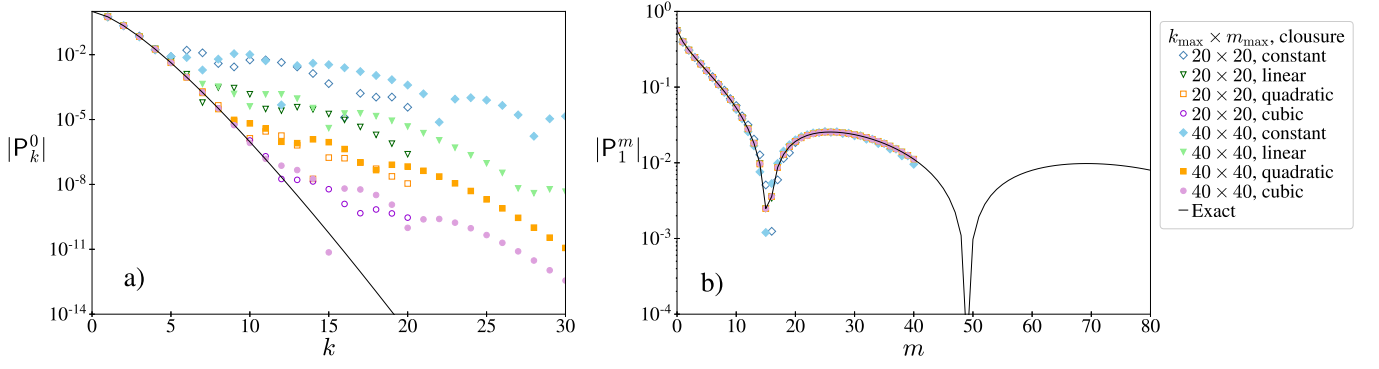


FIG. 2. Absolute value of the Fourier-Hermite modes $|P_k^m|$ in the PS state for $\varepsilon = 1.8$. The exact results are depicted as a solid line. Symbols correspond to modes obtained from a truncation of Eq. (18) with the configurations indicated in the label at the right-hand side. (a) Constant $m = 0$, (b) Constant $k = 1$.

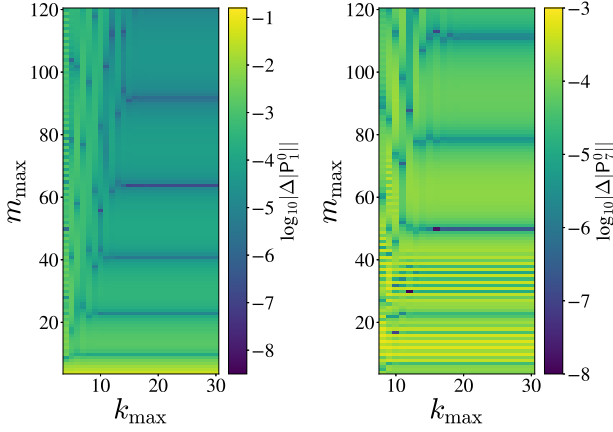


FIG. 3. Level plot of the error of $|P_1^0|$ (left) and $|P_7^0|$ (right) as a function of k_{\max} and m_{\max} , for the linear closure (15). The scale is logarithmic, see color bar adjacent to each panel. The KM is in the state of PS with $\varepsilon = 1.8 > \varepsilon_c$. The exact values of the modes are $|P_1^0| = 0.563\dots$ and $|P_7^0| = 1.79\dots \times 10^{-4}$.

V. KURAMOTO MODEL WITH BIMODAL DISTRIBUTION

The main goal of this section, and the next one, is to illustrate the practicality of the Fourier-Hermite modes with a couple of systems poorly described through a brute-force numerical integration of the oscillator ensembles.

The KM with bi-modal frequency distribution is a classical problem^{23,32}. With the advent of the Ott-Antonsen theory, the problem became (almost) fully solvable for frequency distributions of rational type, see e.g.^{33–36}. Instead, we consider here a distribution equal to the sum of two normal distributions centered at $\pm\Omega_0$ and variance σ^2 . Individual natural frequencies Ω_j are distributed as: $\Omega_j \sim [\mathcal{N}(\Omega_0, \sigma^2) + \mathcal{N}(-\Omega_0, \sigma^2)]/2$. This distribution, bimodal only if $\Omega_0 > \sigma$, was previously studied in Ref.³³. There, several domain boundaries in the phase diagram were determined imprecisely,

since they were obtained from simulations with $N = 10000$ oscillators. This problem is a good example to demonstrate the potential of the Fourier-Hermite moments.

For convenience, we reformulate the system as a two-population problem, i.e. as two populations with Gaussian frequency distributions centered at $\pm\Omega_0$ with variance σ^2 . Denoting the phases of each subpopulation as θ_j^+ and θ_j^- , we can write the ODEs governing the system as:

$$\dot{\theta}_j^\pm = \sigma\omega_j \pm \Omega_0 + \varepsilon R \sin(\Psi - \theta_j^\pm), \quad (23)$$

where $Z_1 \equiv R e^{i\Psi}$ is the average over the order parameters of each subpopulation: $Z_1 = (Z_1^+ + Z_1^-)/2$. We introduce two sets of Fourier-Hermite modes, P_k^m and Q_k^m , for the subpopulations centered at Ω_0 and $-\Omega_0$, respectively. After a straightforward calculation, cf. (18), we obtain the evolution equation of each set:

$$\frac{1}{k} \dot{P}_k^m = i\Omega_0 P_k^m + f(Z_1, P_{k\pm 1}^{m\pm 1}), \quad (24a)$$

$$\frac{1}{k} \dot{Q}_k^m = -i\Omega_0 Q_k^m + f(Z_1, Q_{k\pm 1}^{m\pm 1}), \quad (24b)$$

where the function f is a shorthand notation for

$$f(Z_1, P_{k\pm 1}^{m\pm 1}) = \sigma \left(\sqrt{m} P_k^{m-1} - \sqrt{m+1} P_k^{m+1} \right) + \frac{\varepsilon}{2} \left(P_{k+1}^m Z_1^* - P_{k-1}^m Z_1 \right). \quad (25)$$

The identity $Z_1 = (P_1^0 + Q_1^0)/2$ closes the system of equations.

In Fig. 4 we show the phase diagram of the model. For ease of comparison, the scaling of the axes is identical to Fig. 6 in³³. The model exhibits three different behaviors: the uniform incoherent state (UIS), partial synchronization (PS), and standing wave (SW). The latter state corresponds to two counter-rotating clusters of phase-locked oscillators. Moreover, two adjacent regions of bistability exist: UIS/PS and SW/PS. Solid lines in black and grey constitute the stability boundary of UIS, and they correspond to (circle-)pitchfork, and (degenerate) Hopf bifurcations, respectively. These lines are obtained analytically, and are therefore identical to those in Ref.³³.

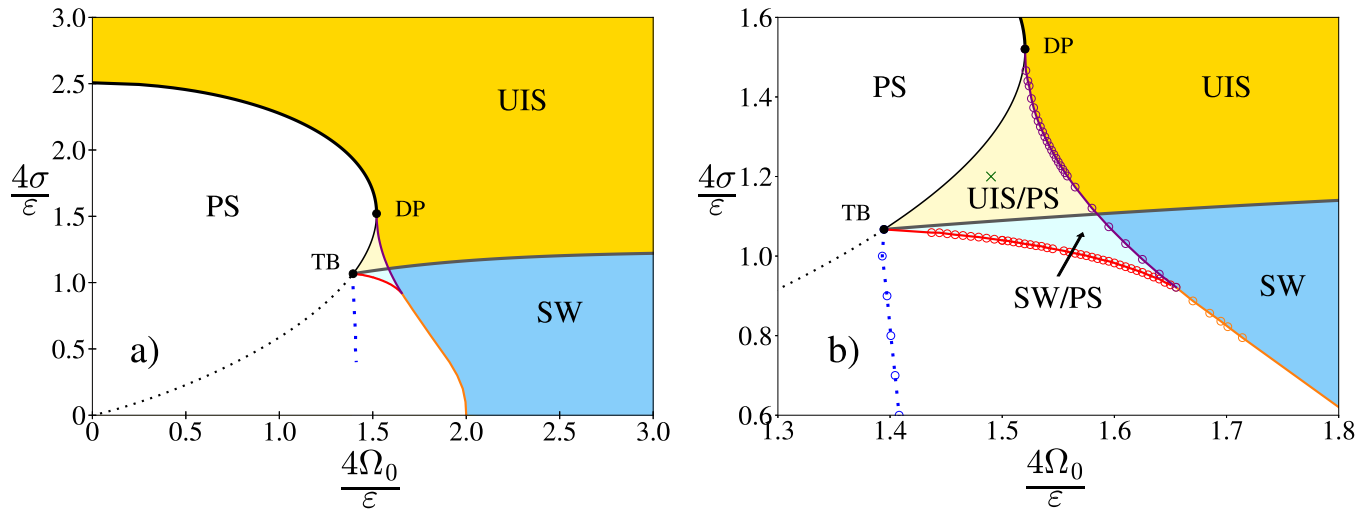


FIG. 4. (a) Phase diagram of the KM with bi-Gaussian frequency distribution. The domains of UIS and SW are shaded in yellow and cyan, respectively. Light shading is used to signify coexistence with PS. The black lines indicate the locus of the circle-pitchfork bifurcation of incoherence. The solid style is used when an attractor is involved in the bifurcation; the thick (thin) line correspond to the super- (sub-) critical bifurcation of UIS. The gray line is the locus of a (degenerate) Hopf bifurcation, UIS \rightarrow SW transition. Both circle-pitchfork and Hopf lines are computed analytically. The pitchfork bifurcation line has a closed expression $\tilde{\Omega}_0^2 = -2\tilde{\sigma}_p^2 \ln(\tilde{\sigma}_p/\sqrt{2\pi})$, with $\tilde{\sigma} = 4\sigma/\varepsilon$, and $\tilde{\Omega}_0 = 4\Omega_0/\varepsilon$. Codimension-2 points DP (degenerate pitchfork), and TB (Takens-Bogdanov) fall on top of this line at $\tilde{\sigma} = \tilde{\Omega}_0 = 1.52035\dots$, and at $\tilde{\sigma} = 1.06706\dots$, respectively. The purple, red, and orange solid lines correspond to numerical estimations, via Eq. (24), of saddle-node, SNIC and homoclinic bifurcations, respectively. A third codimension-2 point is found at the coalescence of the saddle-node and the homoclinic lines. Dotted lines correspond to bifurcations involving unstable states only. In particular, the blue dotted line is the (partial) locus of a drift-pitchfork bifurcation at which mirror traveling waves annihilate. (b) Magnification of the bistability regions in panel (a). Numerical data are depicted as empty circles. The cross in the UIS/PS region indicates the parameter values used in Fig. 5.

In contrast, the colored solid lines in Fig. 4 can only be obtained numerically. They correspond to standard saddle-node (purple), saddle-node on the invariant circle (SNIC, orange), and homoclinic (red) bifurcations. The location of these lines is remarkably improved with respect to Ref.³³. Our numerical simulations were carried out with $k_{\max} = m_{\max} = 20$ and a fourth order Runge-Kutta scheme with step size $\Delta t = 0.01$. For $4\sigma/\varepsilon < 0.3$, $|P_1^0|$ and $|Q_1^0|$ approach 1, and we had to increase the number of modes up to $k_{\max} = m_{\max} = 40$ in order to fully delineate the SNIC line. The results perfectly match with the location of the codimension-two points, degenerate pitchfork (DP) and Takens-Bogdanov (TB), which are known analytically. This implies that the thermodynamic limit of (23) is essentially achieved with at most $(2 \times 2 \times 40 \times 41 =)$ 6560 degrees of freedom. Actually, $(2 \times 2 \times 20 \times 21 =)$ 1680 degrees of freedom are generally enough to capture the thermodynamic limit. The simulation of the Fourier-Hermite modes does not suffer of finite-size fluctuations, in contrast to simulating ensembles of phase oscillators. Moreover, the evolution equations are purely algebraic, in contrast to the computationally expensive trigonometric interaction functions of the oscillator ensemble.

Another advantage of the moment-based approach is that it allows us to track unstable PS states and unstable traveling waves. The traveling wave solution corresponds to a solid rotation, $P_k^m(t) = p_k^m e^{ik\Omega t}$, $Q_k^m(t) = q_k^m e^{ik\Omega t}$, where the angular velocity Ω is one additional unknown. After inserting this solution into Eq. (24), the unknowns p_k^m , q_k^m , and Ω are found via

a Newton-Raphson algorithm (imposing $p_1^0 \in \mathbb{R}^+$). Moreover, the linear stability of both, PS and traveling waves, can be accurately determined linearizing the system (for the traveling wave one has to adopt a rotating reference frame at frequency Ω). In the model investigated in this section, the previous procedure permitted us to find the locus of a drift-pitchfork bifurcation. A part of its locus is indicated by blue dotted line in Fig. 4. It is absent in the phase diagram presented in Ref.³³, as there is not an obvious manner of observing these unstable solutions simulating an ensemble of oscillators. At the drift-pitchfork bifurcation, twin unstable traveling waves (born at the Hopf bifurcation) cease to exist, via collision with an unstable PS state. An equivalent bifurcation line was recently detected for a distribution sum of two Lorentzians³⁶, although (mistakenly) labeled as a saddle-node bifurcation. As the drift-pitchfork line does not involve any attractors we did not made more efforts to trace it completely. In analogy to the result in³⁶, we expected this line to bend backwards and terminate at the origin. The presence of a drift-pitchfork bifurcation confirms that the TB point fully consistent with the $O(2)$ symmetry of the model: invariance under rotation $\theta \rightarrow \theta + c$ and reflection $\Omega \rightarrow -\Omega$. In particular, the $O(2)$ -symmetric Takens-Bogdanov observed corresponds to the scenario “IV-” in the nomenclature of Ref.³⁷, where the codimension-2 bifurcation was fully unfolded.

We conclude this section with a simple numerical experiment. Our intention is to show the limitations of working directly with populations of oscillators. We take 5000 os-

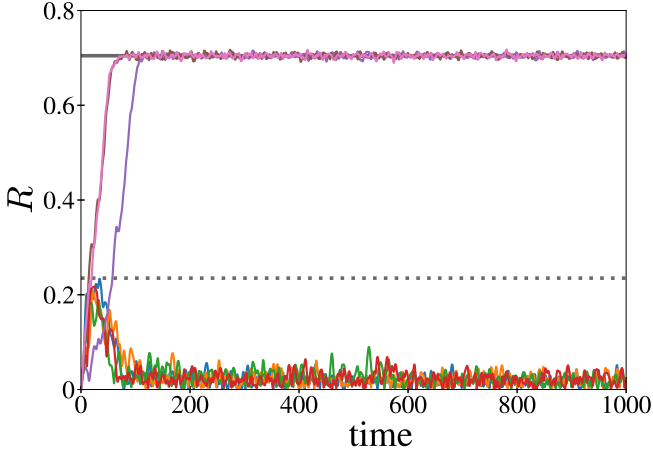


FIG. 5. Time evolution of $R(t)$ for $N = 5000$ oscillators and 7 different initial conditions with random initial phases. The parameter values correspond to the cross in Fig. 4(b), inside the bistability region UIS/PS, with $\sigma = 1$. Stable and unstable PS states correspond to fixed points of Eq. (24), and they are shown as thick grey lines in solid and dashed styles, respectively.

oscillators with the parameter values indicated by the cross in Fig. 4(b). Incoherence is stable, and coexists with PS. Hence, starting the oscillators in a (finite-size version) of the UIS should not be particularly interesting. To our surprise, even if the phases are initiated at random, the system may jump to the PS state. After a surprising initial upstroke of R , 3 out of 7 realizations ended at the PS state, see Fig. 5. In this figure, it is manifest the role of the unstable PS state, obtained from the moment system, as a threshold in the dynamics. Needless to say that the moment system (24) is much more robust describing the thermodynamic limit, due to the lack of fluctuations. For the same parameter values, incoherence, $P_k^m = Q_k^m = \delta_{k,0} \delta_{m,0}$, is a stable fixed point for any truncation in k and m .

VI. ENLARGED KURAMOTO MODEL

In this section, we apply the moment-based approach to a population of phase oscillators with nonpairwise interactions: the ‘enlarged KM’. This system was recently investigated in Ref.⁶. Our purpose here is to explore the $\sigma \rightarrow 0$ limit of the model, and the convergence of the Lyapunov exponent as $N \rightarrow \infty$ in a regime of collective chaos. We start writing the coupling function:

$$G(\theta, t) = \varepsilon \eta R \sin(\Psi - \theta_j + \alpha) + \frac{\varepsilon^2 \eta^2}{4} \left[R \sin(\Psi - \theta_j + \beta) - R^2 \sin(2\Psi - 2\theta_j + \beta) + R Q \sin(\Phi - \Psi - \theta_j) \right]. \quad (26)$$

Two mean fields enter in this equation $Z_1 \equiv R e^{i\Psi}$, and the second Kuramoto-Daido order parameter $Z_2 \equiv Q e^{i\Phi}$. In contrast to other models with nonpairwise interactions, see e.g.^{38–40},

the enlarged KM is not simply postulated. It is obtained applying phase reduction⁴¹ to a population of Stuart-Landau oscillators, up to second order in the coupling constant ε . Constants η , α and β in Eq. (26) depend on the original constants c_1 and c_2 via $\eta \equiv \sqrt{(1+c_2^2)(1+c_1^2)}$, $\alpha \equiv \arg[1+c_1c_2+(c_1-c_2)i]$, and $\beta \equiv \arg(1-c_1^2+2c_1i)$. For completeness, we write the ODE governing the Stuart-Landau oscillators. In this way, we can understand the meaning of c_1 and c_2 (related to reactivity and shear, respectively):

$$\dot{A}_j = (1+i\sigma\omega_j)A_j - (1+ic_2)|A_j|^2A_j + \varepsilon(1+ic_1)(\bar{A} - A_j), \quad (27)$$

where $\bar{A} = N^{-1} \sum_j A_j$.

In a previous work⁶, we showed that Eq. (26) reproduces the rich phenomenology of the ensemble of Stuart-Landau oscillators at weak coupling. In contrast, the first-order phase approximation, neglecting powers of ε above or equal to 2, only predicts two different collective states: UIS and PS. The enlarged KM cannot be analyzed within the Ott-Antonsen theory, because of the second harmonic in θ in the interaction function. This means that no low-dimensional description is available, irrespective of the frequency distribution. As we will show below, under weak coupling and weak heterogeneity ($\sigma \ll 1$, $0 < \varepsilon \ll 1$) the study of the model through direct numerical simulations is impractical. Apart from the unavoidable finite-size fluctuations, the dynamics turns out to be very slow, and long transients are needed to reach stationary regimes. Possessing an efficient numerical scheme becomes essential. We resort to the Fourier-Hermite modes to explore the dynamics of the enlarged KM with Gaussian heterogeneity. After, straightforward calculations we obtain the evolution equations of the moments P_k^m :

$$\begin{aligned} k^{-1} \dot{P}_k^m = & \sigma \left(\sqrt{m} P_k^{m-1} - \sqrt{m+1} P_k^{m+1} \right) \\ & + \frac{\varepsilon \eta}{2} \left(P_{k-1}^m Z_1 e^{i\alpha} - P_{k+1}^m Z_1^* e^{-i\alpha} \right) \\ & + \frac{\varepsilon^2 \eta^2}{8} \left(P_{k-1}^m Z_1 e^{i\beta} - P_{k+1}^m Z_1^* e^{-i\beta} - P_{k-2}^m Z_1^2 e^{i\beta} \right. \\ & \left. + P_{k+2}^m Z_1^{*2} e^{-i\beta} + P_{k-1}^m Z_2 Z_1^* - P_{k+1}^m Z_2^* Z_1 \right), \quad (28) \end{aligned}$$

where $Z_1 = P_1^0$ and $Z_2 = P_2^0$. These equations were integrated using the fourth order Runge-Kutta method with time step $\Delta t = 0.01$.

A. Phase diagram

We start reviewing the phase diagram obtained in Ref.⁶. Figure 6 shows a partial phase diagram for specific values of the parameters $c_2 = 3$ and $\sigma = 10^{-3}$. A couple of bifurcation lines are omitted to simplify the presentation. In the yellow region UIS is stable. Crossing the black line stability is transferred to a partially synchronized state (PS). Interestingly, the blue line indicates the locus of a secondary instability where PS itself becomes unstable through a Hopf bifurcation. The

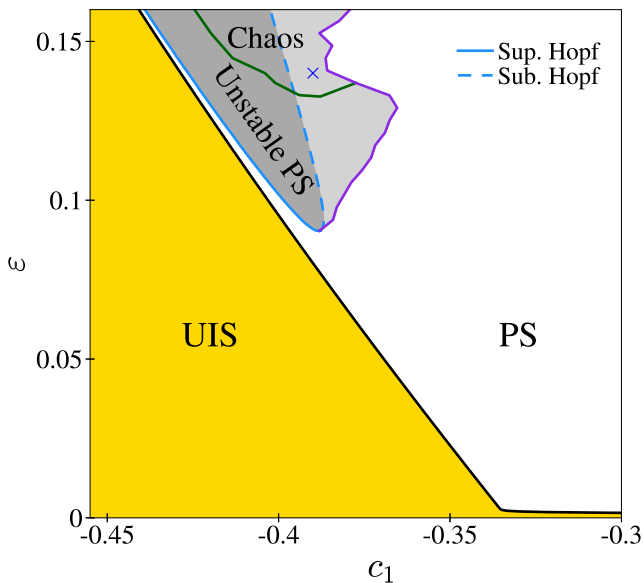


FIG. 6. Partial phase diagram obtained for the interaction function (26), with for $c_2 = 3$ and $\sigma = 10^{-3}$. Yellow and white regions indicate stable UIS and stable PS, respectively. At the solid (dashed) blue line PS undergoes a supercritical (subcritical) Hopf bifurcation. In the light grey shaded region PS and more complex (unsteady) dynamics coexist. The green line bounds the chaotic domain inside the unsteady-dynamics region.

linear stability of PS was calculated finding the rotating solution $\mathbf{P}_k^m(t) = \mathbf{p}_k^m e^{ik\Omega t}$, as with the traveling wave in the previous section, and evaluating the eigenvalue of the Jacobian with the largest real part in the corotating frame. Hence, PS is unstable inside the dark shaded region of Fig. 6. This instability is only possible thanks to the last two terms in Eq. (26), which confer three-body phase interactions to the model. Hence, in the shaded region, the meanfield dynamics display complex oscillations. In particular, above the green line the dynamics becomes chaotic (or hyperchaotic), see⁶. The chaoticity is characterized calculating the Lyapunov exponents of the dynamical system (28). We end this overview noting that in the light shaded region there is bistability between PS and unsteady dynamics (chaotic or not).

It is important to stress that obtaining Fig. 6 was possible thanks to the use of the Fourier-Hermite modes \mathbf{P}_k^m , with a maximal size of $k_{\max} = m_{\max} = 40$. Performing direct numerical simulations it would be virtually impossible to achieve such a level of detail in the phase diagram. In particular, to validate the existence of collective chaos is particularly difficult, see below.

B. The homogeneous limit ($\sigma \rightarrow 0$)

The case $\sigma = 0$ was studied in⁴¹. That system only exhibits UIS, full synchrony, and an intermediate region with nonuniform incoherent states ($Z_1 = 0$, $|Z_2| \equiv Q = \text{const.} > 0$). There is not a correspondence between $\sigma = 0$ and $\sigma > 0$. While, full

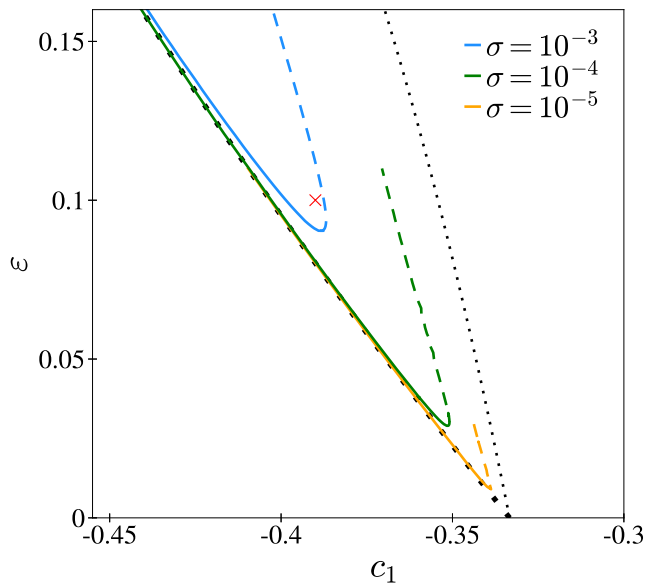


FIG. 7. Location of Hopf bifurcation for $c_2 = 3$ and $\sigma = 10^{-3}, 10^{-4}, 10^{-5}$ in blue, green and orange respectively. The lines were obtained using (28) with $k_{\max} = m_{\max} = 40$. The right boundary is not completely depicted because an extraordinary large number of modes would be needed to calculate it. The black dotted lines are the stability boundaries of UIS (left) and full synchrony (right) for $\sigma = 0$. The red cross indicates the parameter values used in Fig. 8.

synchrony is the limit of PS, it is not obvious how nonuniform incoherent states may appear as σ is lowered to 0. Next, we use the Fourier-Hermite modes to understand the limit $\sigma \rightarrow 0$.

In Fig. 7 we show the stability boundary of PS for three different σ values. Let us emphasize that finding those three boundaries from direct numerical simulations of an ensemble of oscillators would be virtually impossible, specially considering small values of σ and ε achieved. We may see that as σ decreases, the tip of the boundary progressively approaches the abscissa at $c_1 = -1/3$. We conclude that as soon as σ becomes nonzero the Hopf bifurcation appears making the $\sigma \rightarrow 0$ limit singular. The left (right) black dotted line in the figure is the stability boundary of UIS (full synchrony) for $\sigma = 0$. From the figure we infer that the supercritical Hopf bifurcation of PS collides with UIS boundary in the limit $\sigma \rightarrow 0$. Complementary, the subcritical branch becomes the stability boundary of full synchrony. This is consistent because bistability is also observed in the $\sigma = 0$ case⁴¹.

The previous discussion, at the level of bifurcations, is not saying us anything about how is the system behaving as $\sigma \rightarrow 0$. In Figs. 8(a) and 8(b) the time evolution of $R(t)$ and $Q(t)$ are depicted for $\sigma = 10^{-4}$ and 10^{-5} , respectively. The remaining parameter values are the same in both panels, and correspond to the red cross included in Fig. 7. The model displays slow-fast dynamics. The mean field R remains close to 0 most of the time, while Q exhibits a slow decay, followed by a rapid increase. The different time scale in both panels indicates that the slow time scale is diverging as $\sigma \rightarrow 0$. Moreover the range of Q decreases, and (slowly) approaches the asymp-

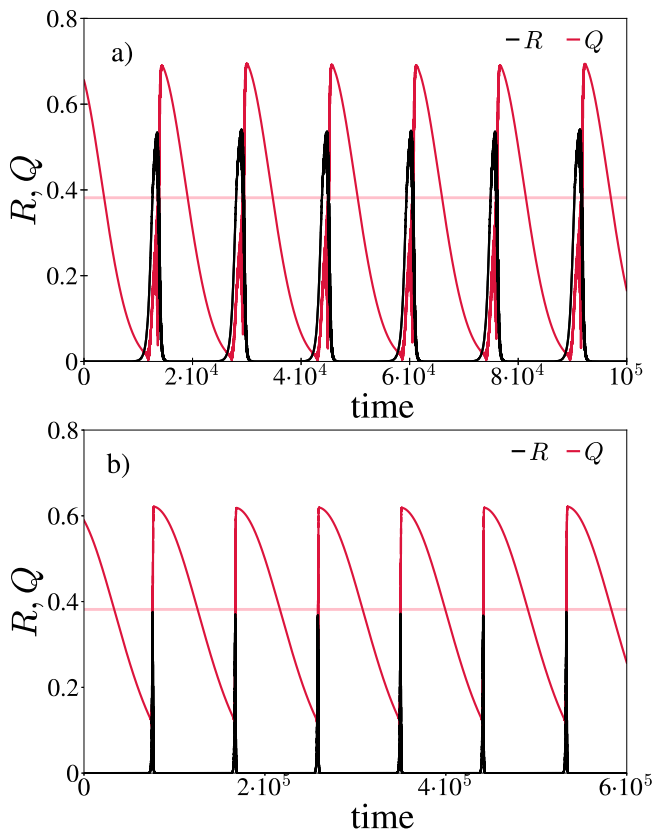


FIG. 8. Dynamics of the enlarged KM for (a) $\sigma = 10^{-4}$ and (b) $\sigma = 10^{-5}$. The time series are the result of integrating Eq. (28) with $c_1 = -0.39$ and $\varepsilon = 0.1$ (see the red cross in Fig. 7). The horizontal pink line is the value of Q in the limit $\sigma = 0$, see Eq. (27) in Ref.⁴¹. Note the different time scale of both panels.

otic value for $\sigma = 0^{41}$, indicated by a pink horizontal line.

C. Collective chaos

In sharp contrast to the standard KM and other models of phase oscillators, the enlarged KM—defined by Eqs. (1) and (26)—exhibits collective chaos with a unimodal distribution of the natural frequencies. Figure 6 shows the location of the chaotic region for particular values of $\sigma = 10^{-3}$ and $c_2 = 3$. In order to determine the boundary of chaos in Fig. 6, we needed to determine the largest Lyapunov exponent in the thermodynamic limit. Again, integrating a finite number of phase oscillators is quite unproductive, due to the ubiquitous microscopic phase chaos⁴, which yields a macroscopic amount, i.e. $O(N)$, of positive Lyapunov exponents (not shown). In contrast, the Fourier-Hermite moments do not suffer of microscopic phase chaos. It is therefore possible to fully characterize the collective chaos of the enlarged KM, and to determine its boundary.

We present next, a numerical test supporting our previous assertions for a specific set of parameters: $c_2 = 3$, $c_1 = -0.39$, $\varepsilon = 0.14$, and $\sigma = 10^{-3}$, see the blue cross in Fig. 6. For these parameter values two stable states coexist in the thermody-

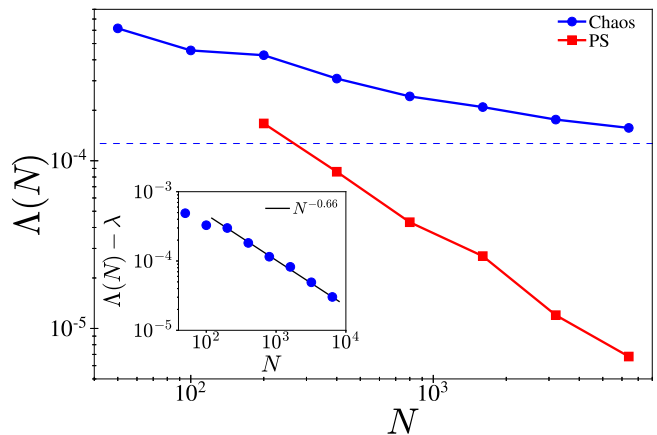


FIG. 9. Largest Lyapunov exponent Λ as function of the population size N for the enlarged KM and two different coexisting states. The values of $\{\omega_j\}_{j=1,\dots,N}$ were selected deterministically to represent the Gaussian distribution (2). The parameter values are those marked by a blue cross in Fig. 6. Circles and squares correspond, respectively, to the states of collective chaos and PS in the thermodynamic limit. The value of the largest Lyapunov exponent $\lambda_1 = \lambda$, obtained from the moment system (28) in the chaotic state, is indicated by a horizontal dashed line. The inset shows a log-log plot of the distance to the asymptotic Lyapunov exponent λ vs. the system size N . The linear fitting, depicted by a solid line, was performed considering points with $N \geq 200$. Note that λ is not a fitting parameter.

amic limit: collective chaos and PS. In the chaotic state the Lyapunov spectrum, obtained linearizing (28) and applying Bennetin's algorithm, is $\{\lambda_n\}_{n=1,2,\dots} = \{1.26 \times 10^{-4}, 6.31 \times 10^{-5}, 1.38 \times 10^{-5}, 0, \dots\}$. This spectrum contains three positive Lyapunov exponents, indicating collective hyperchaos. This means that, for a sufficiently large ensemble, the positive part of the Lyapunov spectrum will consist of three exponents neatly above zero, supplemented by a quasi-continuous set of exponents of $O(N)$ size (whose values approach zero as $N \rightarrow \infty$).

Now, we turn our view to the results obtained from direct numerical simulations with N oscillators. In Fig. 9 we represent the largest Lyapunov exponent Λ as a function of N for each of the coexisting states (PS and collective chaos). In both cases the Lyapunov exponent decreases as N grows. For PS we find a clean decay to zero as $\Lambda(N) \sim 1/N$. This behavior is known for the UIS in the KM⁴ (logarithmic corrections may be present depending on the sampling procedure of the natural frequencies⁴²), and it can be arguably expected for PS too. In the state of collective chaos, the decrease of $\Lambda(N)$ appears to saturate at a finite value consistent with $\lambda \equiv \lambda_1 = 1.26 \times 10^{-4}$, obtained from the Fourier-Hermite modes. To further confirm this guess, we represent in log-scale $\Lambda(N) - \lambda$ vs. N in the inset of Fig. 9. The data are fully consistent with a power-law convergence $\Lambda(N) - \lambda \propto N^{-\gamma}$. The exponent γ , estimated by a linear fit, turns out to be nontrivial: $\gamma \simeq 0.66$. Further work is needed to assess whether and how the value of γ depends on parameters.

VII. CONCLUSIONS AND OUTLOOKS

In this work, we have studied a moment-based approach for ensembles of globally coupled phase oscillators with Gaussian distributed natural frequencies. Several truncations and polynomial closures of the moment system have been tested in the KM. For the index m (related to the decomposition of the oscillator density in the frequency variable), the linear closure is readily implemented, and apparently reliable in all analyzed cases.

The moment-based approach allows us to describe the collective dynamics of an infinite population with a relatively small number of ODEs, avoiding in this way finite-size fluctuations, inherent to direct numerical simulations. Within this framework numerical continuation of PS states is possible, irrespective of their stability. Moreover, linear stability analysis and the computation of “collective” Lyapunov exponents become simple tasks.

We have applied the moment-based approach, specifically Fourier-Hermite modes, to two problems. The first one, the KM with a frequency distribution given by the sum of two Gaussians, previously considered in³³. Here, using moment-based dynamics we have refined the phase diagram in³³, obtaining the accurate loci of bifurcations. Moreover, a new bifurcation line (drift-pitchfork) has been detected, completing the picture around the Takens-Bogdanov point.

The second problem addressed in this work is a complicated phase model, the enlarged KM, derived via second-order phase reduction from an ensemble of Stuart-Landau oscillators. For this system, we have focused on asymptotic properties hardly discernible with direct simulations of large ensembles. First, we have examined the change of the stability boundary of PS as the heterogeneity becomes less and less pronounced ($\sigma \rightarrow 0$). We found the convergence to two stability boundaries analytically known for $\sigma = 0$ ⁴¹. The limit $\sigma \rightarrow 0$ is singular, yet consistent. For small σ the system displays slow-fast dynamics, with the duration of the slow phase diverging as $\sigma \rightarrow 0$. In second place, we investigated the state of collective chaos and the (power-law) convergence of the largest Lyapunov exponent $\Lambda(N)$ with the size. The knowledge of the asymptotic value λ from the moment-based simulation was crucial to estimate the exponent $\gamma \simeq 0.66$ of the power-law behavior: $\Lambda(N) - \lambda \sim N^{-\gamma}$.

Our presentation is limited to the simplest situations. We provide next a list of manners in which the moment-based approach can be extended:

1. We have restricted to Gaussian heterogeneity. Other distributions $\tilde{g}(\omega)$ with finite moments can be analyzed using their corresponding sets of orthonormal polynomials $\{\tilde{h}_m(\omega)\}_{m=0,1,\dots}$, satisfying $\int \tilde{h}_m(\omega)\tilde{h}_n(\omega)\tilde{g}(\omega)d\omega = \delta_{m,n}$. Each set of orthonormal polynomials satisfies a specific recurrence relation: $\omega\tilde{h}_m(\omega) = b_m\tilde{h}_{m+1} + a_m\tilde{h}_m + b_{m-1}\tilde{h}_{m-1}$, leading to a particular variation of Eq. (14). (Note that $a_m = 0$ if $\tilde{g}(\omega)$ is even.) Still, for the specific $\tilde{g}(\omega)$, a preliminary study of the suitable closure(s) should be carried out.
2. We have considered purely deterministic equations.

Adding independent white noises $+\xi_j$ to Eq. (1) does not modify the approach essentially. If the covariance of the noise is $\langle \xi_j(t)\xi_{j'}(t') \rangle = 2D\delta_{j,j'}\delta(t-t')$, then the continuity Eq. (3) gains the term $+D\partial^2\rho/\partial\theta^2$ in the right-hand side (Fokker-Planck equation). This simply results in a new (dissipative) term $-DkP_k^m$ in Eq. (14).

3. In our presentation heterogeneity appears in an additive form, see Eq. (1). The same strategy could be followed, in principle, if multiplicative disorder was present instead. Models of this type include ensembles of theta neurons^{43,44}, generalizations of the KM⁴⁵⁻⁵⁰, and the Winfree model with distributed phase response curves⁵¹.

All in all, we judge the moment-based approach studied in this paper as a very useful tool to investigate the dynamics of ensembles of heterogeneous phase oscillators.

ACKNOWLEDGMENTS

IL acknowledges support by Universidad de Cantabria and Government of Cantabria under the Concepción Arenal programme.

DATA AVAILABILITY

The data that support the findings of this study are available from the corresponding author upon reasonable request.

REFERENCES

- ¹A. T. Winfree, *The Geometry of Biological Time* (Springer, New York, 1980).
- ²Y. Kuramoto, *Chemical Oscillations, Waves, and Turbulence* (Springer-Verlag, Berlin, 1984).
- ³A. Pikovsky and M. Rosenblum, “Dynamics of globally coupled oscillators: Progress and perspectives,” *Chaos* **25**, 097616 (2015).
- ⁴O. V. Popovych, Y. L. Maistrenko, and P. A. Tass, “Phase chaos in coupled oscillators,” *Phys. Rev. E* **71**, 065201(R) (2005).
- ⁵H. Chiba, “Continuous limit and the moments system for the globally coupled phase oscillators,” *Discrete Contin. Dyn. Syst. Ser. A* **33**, 1891–1903 (2013).
- ⁶I. León and D. Pazó, “Enlarged Kuramoto model: Secondary instability and transition to collective chaos,” *Phys. Rev. E* **105**, L042201 (2022).
- ⁷A. S. Pikovsky, M. G. Rosenblum, and J. Kurths, *Synchronization, a Universal Concept in Nonlinear Sciences* (Cambridge University Press, Cambridge, 2001).
- ⁸H. Nakao, “Phase reduction approach to synchronisation of nonlinear oscillators,” *Contemp. Phys.* **57**, 188–214 (2016).
- ⁹D. C. Michaels, E. P. Matyas, and J. Jalife, “Mechanisms of sinoatrial pacemaker synchronization: a new hypothesis,” *Circ. Res.* **61**, 704–714 (1987).
- ¹⁰J. Buck and E. Buck, “Synchronous fireflies,” *Sci. Am.* **234**, 74 (1976).
- ¹¹K. Wiesenfeld, P. Colet, and S. H. Strogatz, “Synchronization transitions in a disordered Josephson series array,” *Phys. Rev. Lett.* **76**, 404–407 (1996).
- ¹²S. H. Strogatz, *Sync: The emerging science of spontaneous order*. (Hyperion Press, New York, 2003).
- ¹³A. T. Winfree, “Biological rhythms and the behavior of populations of coupled oscillators,” *J. Theor. Biol.* **16**, 15–42 (1967).

- ¹⁴Y. Kuramoto, “Self-entrainment of a population of coupled non-linear oscillators,” in *International Symposium on Mathematical Problems in Theoretical Physics*, Lecture Notes in Physics, Vol. 39, edited by H. Araki (Springer, Berlin, 1975) pp. 420–422.
- ¹⁵Y. Kuramoto and D. Battogtokh, “Coexistence of coherence and incoherence in nonlocally coupled phase oscillators,” *Nonlinear Phenom. Complex Syst.* **5**, 380–385 (2002).
- ¹⁶E. Montbrió and D. Pazó, “Kuramoto model for excitation-inhibition-based oscillations,” *Phys. Rev. Lett.* **120**, 244101 (2018).
- ¹⁷K. P. O’Keeffe, H. Hong, and S. H. Strogatz, “Oscillators that sync and swarm,” *Nature communications* **8**, 1–13 (2017).
- ¹⁸S. Chandra, M. Girvan, and E. Ott, “Continuous versus discontinuous transitions in the d -dimensional generalized Kuramoto model: Odd d is different,” *Phys. Rev. X* **9**, 011002 (2019).
- ¹⁹C. Bick, M. Goodfellow, C. R. Laing, and E. A. Martens, “Understanding the dynamics of biological and neural oscillator networks through exact mean-field reductions: a review,” *J. Math. Neurosci.* **10**, 1–43 (2020).
- ²⁰S. H. Strogatz and R. E. Mirollo, “Stability of incoherence in a population of coupled oscillators,” *J. Stat. Phys.* **63**, 613–635 (1991).
- ²¹E. Ott and T. M. Antonsen, “Low dimensional behavior of large systems of globally coupled oscillators,” *Chaos* **18**, 037113 (2008).
- ²²E. Ott and T. M. Antonsen, “Long time evolution of phase oscillator systems,” *Chaos* **19**, 023117 (2009).
- ²³J. A. Acebrón, L. L. Bonilla, C. J. Pérez-Vicente, F. Ritort, and R. Spigler, “The Kuramoto model: A simple paradigm for synchronization phenomena,” *Rev. Mod. Phys.* **77**, 137–185 (2005).
- ²⁴C. J. Perez and F. Ritort, “A moment-based approach to the dynamical solution of the Kuramoto model,” *J. Phys. A: Math. Gen.* **30**, 8095–8103 (1997).
- ²⁵H. Daido, “Critical conditions of macroscopic mutual entrainment in uniformly coupled limit-cycle oscillators,” *Prog. Theor. Phys.* **89**, 929–934 (1993).
- ²⁶H. Sakaguchi, “Cooperative phenomena in coupled oscillator systems under external fields,” *Prog. Theor. Phys.* **79**, 39–46 (1988).
- ²⁷Throughout this work the equivalence between continuous and finite- N formulations is taken for granted (as proven, for example, for the KM in⁵). This is not always the case though. In a model analyzed in³⁹, $\dot{\theta}_j = \sigma\omega_j + \varepsilon R^2 \sin(2\Psi - 2\theta_j)$, incoherence remains unstable for any finite N (and large enough ε), while it is stable in the continuum limit. For finite populations residence times near incoherence diverge with N . Such, perhaps pathological, situations require a careful analysis and are ignored hereafter.
- ²⁸S. Shinomoto and Y. Kuramoto, “Phase Transitions in Active Rotator Systems,” *Prog. Theor. Phys.* **75**, 1105–1110 (1986).
- ²⁹H. Hong, H. Chaté, H. Park, and L.-H. Tang, “Entrainment transition in populations of random frequency oscillators,” *Phys. Rev. Lett.* **99**, 184101 (2007).
- ³⁰H. Hong, H. Chaté, L.-H. Tang, and H. Park, “Finite-size scaling, dynamic fluctuations, and hyperscaling relation in the Kuramoto model,” *Phys. Rev. E* **92**, 022122 (2015).
- ³¹This condition can be expressed in terms of the modified Bessel functions $1 = \varepsilon \sqrt{\frac{\pi}{8}} e^{-R^2 \varepsilon^2 / 4} \left[I_0 \left(\frac{R^2 \varepsilon^2}{4} \right) + I_1 \left(\frac{R^2 \varepsilon^2}{4} \right) \right]$.
- ³²S. H. Strogatz, “From Kuramoto to Crawford: exploring the onset of synchronization in populations of coupled oscillators,” *Physica D* **143**, 1–20 (2000).
- ³³E. A. Martens, E. Barreto, S. H. Strogatz, E. Ott, P. So, and T. M. Antonsen, “Exact results for the Kuramoto model with a bimodal frequency distribution,” *Phys. Rev. E* **79**, 026204 (2009).
- ³⁴D. Pazó and E. Montbrió, “Existence of hysteresis in the Kuramoto model with bimodal frequency distributions,” *Phys. Rev. E* **80**, 046215 (2009).
- ³⁵B. Pietras, N. Deschle, and A. Daffertshofer, “First-order phase transitions in the Kuramoto model with compact bimodal frequency distributions,” *Phys. Rev. E* **98**, 062219 (2018).
- ³⁶S. Guo, Y. Xie, Q. Dai, H. Li, and J. Yang, “Dynamics in the Sakaguchi-Kuramoto model with bimodal frequency distribution,” *PLOS ONE* **15**, 1–13 (2020).
- ³⁷G. Dangelmayr and E. Knobloch, “The Takens-Bogdanov bifurcation with O(2)-symmetry,” *Philos. Trans. Royal Soc. A* **322**, 243–279 (1987).
- ³⁸T. Tanaka and T. Aoyagi, “Multistable attractors in a network of phase oscillators with three-body interactions,” *Phys. Rev. Lett.* **106**, 224101 (2011).
- ³⁹M. Komarov and A. Pikovsky, “Finite-size-induced transitions to synchrony in oscillator ensembles with nonlinear global coupling,” *Phys. Rev. E* **92**, 020901(R) (2015).
- ⁴⁰P. S. Skardal and A. Arenas, “Abrupt desynchronization and extensive multistability in globally coupled oscillator simplexes,” *Phys. Rev. Lett.* **122**, 248301 (2019).
- ⁴¹I. León and D. Pazó, “Phase reduction beyond the first order: The case of the mean-field complex Ginzburg-Landau equation,” *Phys. Rev. E* **100**, 012211 (2019).
- ⁴²M. Carlu, F. Ginelli, and A. Politi, “Origin and scaling of chaos in weakly coupled phase oscillators,” *Phys. Rev. E* **97**, 012203 (2018).
- ⁴³T. B. Luke, E. Barreto, and P. So, “Complete classification of the macroscopic behavior of a heterogeneous network of theta neurons,” *Neural Comput.* **25**, 3207–3234 (2013).
- ⁴⁴T. B. Luke, E. Barreto, and P. So, “Macroscopic complexity from an autonomous network of networks of theta neurons,” *Front. Comput. Neurosci.* **8** (2014), 10.3389/fncom.2014.00145.
- ⁴⁵H. Hong and S. H. Strogatz, “Kuramoto model of coupled oscillators with positive and negative coupling parameters: An example of conformist and contrarian oscillators,” *Phys. Rev. Lett.* **106**, 054102 (2011).
- ⁴⁶E. Montbrió and D. Pazó, “Shear diversity prevents collective synchronization,” *Phys. Rev. Lett.* **106**, 254101 (2011).
- ⁴⁷D. Pazó and E. Montbrió, “The Kuramoto model with distributed shear,” *EPL (Europhys. Lett.)* **95**, 60007 (2011).
- ⁴⁸E. Montbrió and D. Pazó, “Collective synchronization in the presence of reactive coupling and shear diversity,” *Phys. Rev. E* **84**, 046206 (2011).
- ⁴⁹D. Iatsenko, S. Petkoski, P. V. E. McClintock, and A. Stefanovska, “Stationary and traveling wave states of the Kuramoto model with an arbitrary distribution of frequencies and coupling strengths,” *Phys. Rev. Lett.* **110**, 064101 (2013).
- ⁵⁰D. Iatsenko, P. V. E. McClintock, and A. Stefanovska, “Oscillator glass in the generalized Kuramoto model: synchronous disorder and two-step relaxation,” *Nat. Commun.* **5**, 4188 (2014).
- ⁵¹D. Pazó, E. Montbrió, and R. Gallego, “The Winfree model with heterogeneous phase-response curves: analytical results,” *J. Phys. A: Math. and Theor.* **52**, 154001 (2019).